

# Primordial Magnetism in the CMB: Exact Treatment of Faraday Rotation and WMAP7 Bounds

Levon Pogosian<sup>1</sup>, Amit P.S. Yadav<sup>2</sup>, Yi-Fung Ng<sup>3</sup> and Tanmay Vachaspati<sup>4</sup>

<sup>1</sup>*Department of Physics, Simon Fraser University,  
Burnaby, BC, V5A 1S6, Canada*

<sup>2</sup>*Institute for Advanced Study,  
Princeton, NJ 08540, USA*

<sup>3</sup>*CERCA, Physics Department,  
Case Western Reserve University,  
Cleveland, OH 44106-7079, USA*

<sup>4</sup>*Physics Department, Arizona State University,  
Tempe, AZ 85287, USA*

Faraday rotation induced B-modes can provide a distinctive signature of primordial magnetic fields because of their characteristic frequency dependence and because they are only weakly damped on small scales, allowing them to dominate B-modes from other sources. By numerically solving the full CMB radiative transport equations, we study the B-mode power spectrum induced by stochastic magnetic fields that have significant power on scales smaller than the thickness of the last scattering surface. Constraints on the magnetic field energy density and inertial scale are derived from WMAP 7-year data, and are stronger than the big bang nucleosynthesis (BBN) bound for a range of parameters. Observations of the CMB polarization at smaller angular scales are crucial to provide tighter constraints or a detection.

## I. INTRODUCTION

Many early universe scenarios predict the existence of cosmological magnetic fields and several observational techniques are currently being employed to detect such fields [1, 2]. There are also recent claims for the detection of an inter-galactic magnetic field [3]. With further confirmation and refinement, these observations can be turned into a probe of the fundamental interactions that are necessary to generate a primordial magnetic field and to the physics of the early universe. A primordial magnetic field can also have important implications for the formation of first stars, growth of cosmic structure and the present universe.

Of particular interest to us are magnetogenesis scenarios based on phase transitions such as the electroweak phase transition, when Maxwellian electromagnetism first emerged [4–11]. In this scenario particle physics uncertainties are minimal and magnetogenesis is tightly related to the creation of matter, or “baryogenesis” – the magnitude of the magnetic helicity density is approximately equal to the baryon number density. Since the cosmic number density of baryons is known, the scenario enables a prediction for the magnetic helicity density that is largely independent of the details of the electroweak model. Furthermore, the *left-handed* magnetic helicity is a direct outcome of parity violation present in the electroweak model and, like baryon number, is a remarkable large-scale manifestation of a microscopic symmetry violation.

Non-vanishing helicity has important consequences for the evolution of a magnetic field. Although the field is generated on small scales, magnetic helicity allows for an “inverse cascade” where power is transferred from small to large scales, resulting in magnetic coherence on larger scales. In the case of magnetic fields generated at the electroweak scale, the final coherence scale can be on the parsec to kiloparsec scales [6, 12]. While the coherence scale is large, it is not as large as for fields that might be generated during an inflationary epoch. For purposes of calculating observational signatures, magnetic fields generated at a phase transition are stochastic. An important aim of the present work is to find distinctive observational signatures of magnetic fields that are stochastic on sub-Mpc coherence scales.

Once magnetic fields have been injected into the cosmological plasma, the subsequent evolution is described by magneto-hydrodynamical (MHD) equations in an expanding spacetime. Power on very small length scales is expected to be erased by dissipational mechanisms. Power on very large scales is also suppressed because the magnetic field is injected on microscopic scales and cannot extend to arbitrarily large scales. Hence the spectral distribution of the magnetic field is expected to decay fast on small and large scales and be peaked on some intermediate scale, which is presumably at the parsec to kiloparsec scale. The spectral form of the magnetic field has been investigated recently in some detail in Refs. [13, 14] and the results are schematically depicted in Fig. 1.

On the observational front, magnetic fields within galaxies and clusters of galaxies have been studied for many decades and their origin – cosmological versus astrophysical – remains unsettled, though a hybrid explanation is also

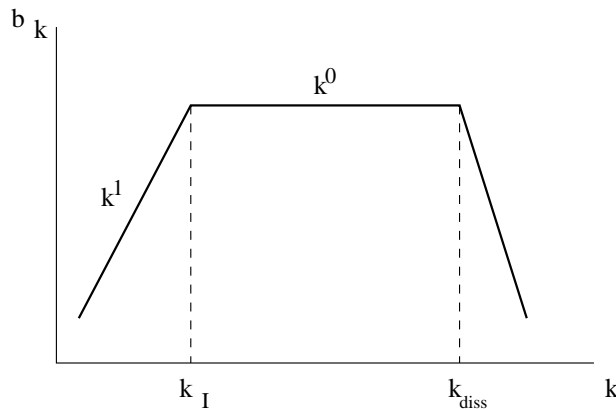


FIG. 1: The Fourier amplitude  $b(k)$  – as given by the square root of the power spectrum – of a stochastic magnetic field generated during a cosmic phase transition is expected to grow for  $k < k_I$  where  $k_I$  is an inertial scale, and obey some other power law for  $k_I < k < k_{\text{diss}}$ , where  $k_{\text{diss}}$  is a dissipative scale. The work of [13] suggests  $k^1$  growth at small  $k$ , then  $k^0$  behavior until  $k_{\text{diss}}$ , beyond which the amplitude falls off very quickly.

conceivable. More recently, observations of TeV gamma ray sources have been used to place *lower* bounds  $\sim 10^{-16}$  G [3, 15–18], and perhaps a measurement  $\sim 10^{-15}$  G [19], on a magnetic field in inter-galactic space,  $\sim 10$  Mpc away from the TeV gamma ray source. It seems likely that such an inter-galactic magnetic field, unassociated with cosmic structure, is primordial, but an astrophysical origin, say based on the expulsion of magnetic fields from active sources, may also be viable.

A detection of magnetic fields in the cosmic microwave background (CMB), for example due to Faraday rotation (FR) of the CMB polarization, would unambiguously point to a cosmological origin because there are no confounding magnetized structures at last scattering. However, an observed FR of the CMB could also be due to magnetic fields along the line of sight, especially within the Milky Way. Hence, it is necessary to find distinctive signatures of FR that occurred at recombination versus that which happened more recently. As we will see, in addition to its characteristic frequency dependence, FR induced B-modes are only weakly damped on small angular scales (high  $\ell$ ), which means they are likely to dominate B-modes from other sources.

Earlier work on FR of the CMB in cosmic magnetic fields has largely focused on the effect of a uniform magnetic field [20, 21] and, when a stochastic magnetic field has been considered, a “thin” LSS was often assumed [22–24]. This approximation results in a tremendous technical simplification but it is not clear if it is suited to study the effects of a magnetic field with coherence scale smaller than the thickness of the LSS. In [25], the finite thickness effects of the LSS were modelled by approximating the visibility function with a Gaussian profile. As we show, the thin LSS approximation is sufficient for order of magnitude estimates, but can be wrong by factors of a few and in an  $\ell$  dependent way.

In the present paper, we study the effect of a primordial magnetic field on the CMB polarization, focussing on the effect of a stochastic field with power on small (sub-Mpc) scales. We calculate the B-mode correlator,  $C_l^{BB}$ , induced by a primordial magnetic field. In the thin LSS approximation of Sec. IV, we show that  $C_l^{BB}$  is directly related to  $C_l^{EE}$  multiplied by the correlation function for the FR,  $C_l^{\alpha\alpha}$ , which we calculate in Sec. III. In Sec. V we move on to our main calculation of  $C_l^{BB}$  with a thick LSS. Here we find that the physics of FR during recombination can be described in terms of “window functions” through which the magnetic field spectrum (see Eq. (65)) appears in  $C_l^{BB}$ . We have to resort to extensive numerical efforts to compute the window functions. Our results are described in Sec. VI. The window functions themselves are independent of the magnetic field power spectrum and are shown in Fig. 2. When the window functions are convolved with the magnetic field power spectrum, we obtain  $C_l^{BB}$ . In Figs. 3, 4 we show the results for  $C_l^{BB}$  for a scale-invariant and a blue magnetic power spectrum. We conclude in Sec. VII. We have made our window functions publicly available at <http://www.sfu.ca/~levon/faraday.html> along with a short Fortran code for calculating  $C_l^{BB}$ .

## II. STOCHASTIC MAGNETIC FIELDS

A statistically homogeneous and isotropic stochastic magnetic field is described by the two-point correlator in Fourier space as

$$\langle b_i(\mathbf{k})b_j(\mathbf{k}') \rangle = (2\pi)^3 \delta^{(3)}(\mathbf{k} + \mathbf{k}') [(\delta_{ij} - \hat{k}_i \hat{k}_j)S(k) + i\varepsilon_{ijl} \hat{k}_l A(k)] , \quad (1)$$

where  $S(k)$  and  $A(k)$ , the symmetric and anti-symmetric magnetic power spectra, are real functions of  $k = |\mathbf{k}|$ . Throughout the paper, we use Gaussian CGS units. The energy density in modes up to some value of  $k$  is given by

$$\epsilon_M(k) = \frac{1}{8\pi} \int_{k' < k} \frac{d^3 k'}{(2\pi)^3} 2S(k') = \frac{1}{(2\pi)^3} \int_0^k dk k^2 S(k). \quad (2)$$

We take the form of  $S(k)$  to correspond to Fig. 1

$$S(k) = \begin{cases} S_* \left(\frac{k}{k_I}\right)^{2n-3}, & 0 < k < k_I \\ S_* \left(\frac{k}{k_I}\right)^{2n'-3}, & k_I < k < k_{\text{diss}} \\ 0, & k_{\text{diss}} < k \end{cases} \quad (3)$$

The results in [13, 26] suggest the exponents  $n = 5/2$  and  $n' = 3/2$ . In our analysis, along with these values, we will also consider the case of a nearly scale invariant spectrum, with  $2n = 2n' = 0.1$ , motivated by an inflationary mechanism of generation of magnetic fields [27, 28].

We will only consider the effect of magnetic field on the CMB for modes with  $l \leq l_{\text{max}} = 10^4$ , as computations at higher  $l$  are very expensive. This corresponds to a minimum comoving scale of 1 Mpc, or  $k_{\text{max}} \sim 1 \text{ Mpc}^{-1}$ . For magnetic fields generated at the electroweak phase transition, the coherence scale is estimated at kpc scales or less [6, 12]. Hence  $k_I$  may be expected to be  $10^3 \text{ Mpc}^{-1}$ . This is much larger than  $k_{\text{max}}$  and thus the  $l \leq 10^4$  modes of the CMB are likely to be affected only by the magnetic field modes in the inertial range  $0 < k < k_I$ , and the form of the power spectrum for  $k > k_I$  plays no direct role. However, even then, the large  $k$  part of the power spectrum would still enter when we derive a constraint on the magnetic field, since the amplitude,  $S_*$ , is fixed by the total energy density in the magnetic field. We now make this point clearer.

First define an “effective magnetic field”,  $B_{\text{eff}}$ , in terms of the total energy density in the magnetic field,  $\epsilon_0$ ,

$$\epsilon_0 \equiv \frac{B_{\text{eff}}^2}{8\pi}. \quad (4)$$

In other words,  $B_{\text{eff}}$  is the field strength of a uniform magnetic field that has the same total energy density as our stochastic magnetic field. Our constraints will be written in terms of  $B_{\text{eff}}$ . To connect to the amplitude of the power spectrum, we first evaluate the energy density in the magnetic field. From Eq. (2) we get

$$\epsilon_M(k) = \begin{cases} \frac{S_* k_I^3}{16\pi^3 n} \left(\frac{k}{k_I}\right)^{2n}, & k \leq k_I \\ \frac{S_* k_I^3}{16\pi^3 n} \left[1 + \frac{n}{n'} \left\{ \left(\frac{k}{k_I}\right)^{2n'} - 1 \right\} \right], & k_I < k \leq k_{\text{diss}} \\ \frac{S_* k_I^3}{16\pi^3 n} \left[1 + \frac{n}{n'} \left\{ \left(\frac{k_{\text{diss}}}{k_I}\right)^{2n'} - 1 \right\} \right], & k_{\text{diss}} < k \end{cases} \quad (5)$$

The total energy density in the magnetic field,  $\epsilon_0$ , is found by setting  $k \rightarrow \infty$ , which is the same as  $\epsilon_M(k)$  for  $k > k_{\text{diss}}$ . Thus, we can write

$$\epsilon_0 = \frac{S_* k_I^3 \kappa}{16\pi^3 n}, \quad (6)$$

where

$$\kappa \equiv 1 + \frac{n}{n'} \left\{ \left(\frac{k_{\text{diss}}}{k_I}\right)^{2n'} - 1 \right\}, \quad (7)$$

and hence

$$B_{\text{eff}} = \frac{1}{\pi} \sqrt{\frac{\kappa S_* k_I^3}{2n}}. \quad (8)$$

For a fixed exponent  $n$ , CMB observations at  $l \leq 10^4$  will only constrain the combination  $S_* k_I^3$ . To then convert the constraint to a bound on the energy density in magnetic fields requires knowledge of the exponent  $n'$  and the inertial and dissipation scales. In other words, the CMB signature for  $l \leq 10^4$  probes the long wavelength tail of the magnetic

spectrum and not the modes where the bulk of the energy density resides. This suggests that it may be favorable to investigate the CMB at yet higher  $l$ ; indeed, our results do show stronger signatures with growing  $l$ .

Big bang nucleosynthesis (BBN) is sensitive to the total energy density in the magnetic field since this is what enters the expansion rate of the universe. The constraint from BBN [29–32] is best expressed in terms of the magnetic field energy density relative to the photon energy density

$$\Omega_{B\gamma} \equiv \frac{\epsilon_0}{\rho_\gamma} \lesssim 10^{-1} \quad (9)$$

The relative density,  $\Omega_{B\gamma}$ , is independent of cosmological epoch since both magnetic field and photon energy density scale as  $a^{-4}$  where  $a(t)$  is the cosmological scale factor. Note that  $\rho_\gamma$  is the photon density which is different from the radiation density at BBN epoch since neutrinos also contribute to radiation.

Finally, all the scaling due to the expansion of the universe can be pulled out by converting to rescaled quantities

$$\mathbf{B}a^2 \rightarrow \mathbf{B}, \quad \rho_\gamma a^4 \rightarrow \rho_\gamma, \quad ka \rightarrow k, \quad (10)$$

and, in what follows, we will use these comoving quantities unless explicitly stated. The final form of the magnetic field power spectrum in the inertial range is

$$S(k) = \Omega_{B\gamma} \rho_\gamma \frac{16\pi^3 n}{\kappa k_I^3} \left( \frac{k}{k_I} \right)^{2n-3}, \quad k < k_I \quad (11)$$

The power spectrum  $S(k)$  will enter the calculation of  $C_l^{BB}$  in combination with powers of  $k$ . So it is convenient to introduce the dimensionless “power spectrum” using powers of  $k$  and also the wavelength of observed radiation,  $\lambda_0$ ,

$$\Delta_M^2(k) \equiv k^3 S(k) \left( \frac{3\lambda_0^2}{16\pi^2 e} \right)^2 = \begin{cases} \Delta_0^2 \left( \frac{k}{k_I} \right)^{2n} & 0 < k < k_I \\ \Delta_0^2 \left( \frac{k}{k_I} \right)^{2n'} & k_I < k < k_{\text{diss}} \\ 0 & k > k_{\text{diss}} \end{cases} \quad (12)$$

where

$$\Delta_0^2 \equiv \frac{9n}{16\pi e^2 \kappa} \rho_\gamma \lambda_0^4 \Omega_{B\gamma} \quad (13)$$

At the present epoch  $\rho_\gamma(t_0) = 4.64 \times 10^{-34} \text{ gm/cm}^3 = 2 \times 10^{-15} (\text{eV})^4$  [33], and so

$$\Delta_0^2 = 1.1 \times 10^4 \frac{\Omega_{B\gamma}}{\kappa} \times \left( \frac{2n}{5} \right) \left( \frac{90 \text{ GHz}}{\nu_0} \right)^4 \quad (14)$$

where we denote the observed CMB frequency by  $\nu_0$ . Note that  $\Delta_0^2$  is independent of  $k_I$ .

In principle,  $k_{\text{diss}}$  is not an independent parameter. One can estimate its value for a given amplitude and shape of the magnetic fields spectrum. According to [34, 35],  $k_{\text{diss}}$  is determined by damping into Alfvén waves and can be related to  $B_{\text{eff}}$  as

$$\frac{k_{\text{diss}}}{1 \text{ Mpc}^{-1}} \approx 1.4 h^{1/2} \left( \frac{10^{-7} \text{ Gauss}}{B_{\text{eff}}} \right), \quad (15)$$

Converting this to  $\Omega_{B\gamma}$ , we obtain

$$k_{\text{diss}} \approx 0.43 \sqrt{\frac{10^{-2} h}{\Omega_{B\gamma}}} \text{ Mpc}^{-1}, \quad (16)$$

where it was useful to know that  $1 \text{ Gauss} = 6.9 \times 10^{-20} \text{ GeV}^2$  when converting between natural units and CGS units. We also note that Eq. (4) implies:

$$B_{\text{eff}} = 3.25 \times 10^{-6} \sqrt{\Omega_{B\gamma}} \text{ Gauss}. \quad (17)$$

The relation (15) is based on the analysis in Ref. [34] where small perturbations on top of a homogeneous magnetic field were treated. To extend this analysis to a stochastic magnetic field with little power on long wavelengths, Ref. [35] introduced a smoothing procedure and split the spectrum into a “homogeneous” part and a “perturbations” part. It is not clear to us if this procedure is valid for an arbitrary spectrum,  $S(k)$ , but we will still use Eq. (15) as an approximate expression for the dissipation scale.

### III. FARADAY ROTATION CORRELATORS

The CMB is linearly polarized and an intervening magnetic field will rotate the polarization vector at a rate given by:

$$d\alpha = \lambda^2 \frac{e^3}{2\pi m_e^2} a n_e \mathbf{B} \cdot d\mathbf{l} , \quad (18)$$

where  $\lambda$  is the wavelength of light,  $a$  is the scale factor normalized so that  $a_{\text{today}} = 1$ ,  $n_e$  is the number density of free electrons,  $d\mathbf{l}$  is the comoving length element along the photon trajectory from the source to the observer and we are using Gaussian natural units with  $\hbar = c = 1$ . Using the known expression for Thomson scattering cross-section,

$$\sigma_T = \frac{8\pi e^4}{3m_e^2} , \quad (19)$$

and integrating along the line of sight, we obtain the Faraday rotation of the polarization angle,

$$\alpha = \frac{3}{16\pi^2 e} \lambda_0^2 \int \dot{\tau}(\mathbf{x}) \tilde{\mathbf{B}} \cdot d\mathbf{l} \quad (20)$$

where  $\dot{\tau}(\mathbf{x}) \equiv n_e \sigma_T a$  is the differential optical depth along the line of sight,  $\lambda_0$  is the observed wavelength of the radiation and  $\tilde{\mathbf{B}} \equiv \mathbf{B} a^2$  is the “comoving” magnetic field. The limits of the integral are from the initial position of the photon to the final position.

FR depends on the free electron density, which becomes negligible towards the end of recombination. Therefore, the bulk of the rotation is produced during a relatively brief period of time when the electron density is sufficiently low for polarization to be produced and yet sufficiently high for the FR to occur. The average FR (in radians) between Thomson scatterings due to a tangled magnetic field was calculated in Ref. [36] and is given by

$$F = \frac{3}{8\pi^2 e} \frac{B_0}{\nu_0^2} \approx 0.08 \left( \frac{B_0}{10^{-9} \text{G}} \right) \left( \frac{30 \text{GHz}}{\nu_0} \right)^2 , \quad (21)$$

where  $B_0$  is the current amplitude of the field and  $\nu_0$  is the radiation frequency observed today.

In this section we will calculate the two-point correlation functions of the FR angle,  $\alpha$ , and this will be related to the two-point correlation function of the magnetic field as given in Eq. (1). The FR correlator will enter the calculation of  $C_l^{BB}$  in the thin LSS approximation of Sec. IV, in which one assumes that all of the polarization was generated at once independently from the FR. In the general case, which we present in Sec. V, the generation of the CMB polarization and its FR are entangled.

FR is sensitive only to the line of sight component of the magnetic field, whereas magnetic helicity, described by the helical power spectrum  $A(k)$  in Eq. (1), depends on all 3 components of the magnetic field. So a correlator of FR cannot be sensitive to the helical properties [22, 37, 38]<sup>1</sup>. Following Ref. [39] without the helical term, we get

$$\langle \alpha(\hat{n}) \alpha(\hat{n}') \rangle = \left( \frac{3\lambda_0^2}{16\pi^2 e} \right)^2 \int \frac{d^3 k}{(2\pi)^3} S(k) \int d\eta \int d\eta' \dot{\tau}(\eta) \dot{\tau}(\eta') e^{-i\mathbf{k} \cdot \hat{n}\eta} e^{+i\mathbf{k} \cdot \hat{n}'\eta'} [\hat{n} \cdot \hat{n}' - (\hat{k} \cdot \hat{n})(\hat{k} \cdot \hat{n}')] \quad (22)$$

where  $\hat{n}$ ,  $\hat{n}'$  are two directions on the sky. Note that, as is conventional, we have written  $\dot{\tau}(\mathbf{x})$  in Eq. (20) as  $\dot{\tau}(\eta)$  in the integrand of Eq. (22) even though  $\mathbf{x} = \hat{n}(\eta_0 - \eta)$ . We have also ignored inhomogeneities in the free electron density along different directions on the sky since this will only give a higher order correction to FR. The limits of the  $\eta$ ,  $\eta'$  integrations are from the time that the photon last scattered to the present time. In general, the last scattering time will be different for different photons but, in the thin LSS approximation, the initial time will be taken to be  $\eta_*$ , the epoch at which the “visibility function”,  $g(\eta) \equiv \dot{\tau} e^{-\tau}$ , is maximum.

Statistical isotropy implies that  $\langle \alpha(\hat{n}) \alpha(\hat{n}') \rangle$  must be a function of  $\hat{n} \cdot \hat{n}'$ . This can also be seen directly by writing Eq. (22) as

$$\langle \alpha(\hat{n}) \alpha(\hat{n}') \rangle = \left( \frac{3\lambda_0^2}{16\pi^2 e} \right)^2 \int \frac{k^2 dk}{(2\pi)^3} S(k) \int d\eta \int d\eta' \dot{\tau}(\eta) \dot{\tau}(\eta') [\hat{n} \cdot \hat{n}' - \partial_{k\eta} \partial_{k\eta'}] \int d^2 \hat{k} e^{-i\mathbf{k} \cdot \hat{n}\eta} e^{+i\mathbf{k} \cdot \hat{n}'\eta'} , \quad (23)$$

---

<sup>1</sup> Indirectly though, helicity does enter the FR signature because magnetic helicity plays a crucial role in the evolution of magnetic fields and the exponent  $n$  in  $S(k)$  (see Eq. (11)).

and using

$$\int d^2\hat{k} e^{-i\mathbf{k}\cdot\hat{n}\eta} e^{+i\mathbf{k}\cdot\hat{n}'\eta'} = 4\pi \sum_l (2L+1) j_L(k\eta) j_L(k\eta') P_L(\hat{n}\cdot\hat{n}') . \quad (24)$$

where  $j_L(x)$  are Bessel functions and  $P_L(x)$  are Legendre polynomials. Hence,  $\langle\alpha(\hat{n})\alpha(\hat{n}')\rangle$  depends only on  $\hat{n}\cdot\hat{n}'$  as expected. As a consequence, the correlator of  $\alpha$ 's can be expanded into Legendre series

$$\langle\alpha(\hat{n})\alpha(\hat{n}')\rangle = \sum_L \frac{(2L+1)}{4\pi} C_L^{\alpha\alpha} P_L(\hat{n}\cdot\hat{n}') \quad (25)$$

and the FR correlators can also be written as  $\langle\alpha_{LM}^* \alpha_{L'M'}\rangle = C_L^{\alpha\alpha} \delta_{LL'} \delta_{MM'}$ , where  $\alpha_{LM}$  are the coefficients in the spherical harmonic decomposition of the FR angle,

$$\alpha(\hat{n}) = \sum_{L,M} \alpha_{LM} Y_{LM}(\hat{n}) . \quad (26)$$

Now combining (23) and (24), and introducing  $j'_L(x) \equiv \partial_x j_L(x)$ , we can write

$$\begin{aligned} \langle\alpha(\hat{n})\alpha(\hat{n}')\rangle &= \left(\frac{3\lambda_0^2}{16\pi^2 e}\right)^2 \frac{2}{\pi} \int k^2 dk S(k) \int d\eta \int d\eta' \dot{\tau}(\eta) \dot{\tau}(\eta') \\ &\times \sum_L \frac{(2L+1)}{4\pi} [(\hat{n}\cdot\hat{n}') P_L(\hat{n}\cdot\hat{n}') j_L(k\eta) j_L(k\eta') - j'_L(k\eta) j'_L(k\eta') P_L(\hat{n}\cdot\hat{n}')] . \end{aligned} \quad (27)$$

Applying the recursion relation

$$(L+1)P_{L+1}(x) = (2L+1)xP_L(x) - LP_{L-1}(x) \quad (28)$$

to the  $(\hat{n}\cdot\hat{n}')P_L(\hat{n}\cdot\hat{n}')$  term in (27) results in

$$\begin{aligned} \langle\alpha(\hat{n})\alpha(\hat{n}')\rangle &= \left(\frac{3\lambda_0^2}{16\pi^2 e}\right)^2 \frac{2}{\pi} \int k^2 dk S(k) \int d\eta \int d\eta' \dot{\tau}(\eta) \dot{\tau}(\eta') \sum_L \frac{(2L+1)}{4\pi} P_L(\hat{n}\cdot\hat{n}') \\ &\times \left[ \frac{L}{2L+1} j_{L-1}(k\eta) j_{L-1}(k\eta') + \frac{L+1}{2L+1} j_{L+1}(k\eta) j_{L+1}(k\eta') - j'_L(k\eta) j'_L(k\eta') \right] . \end{aligned} \quad (29)$$

In analogy with the way  $C_L$ 's are evaluated for CMB, it is convenient to introduce “transfer” functions  $\mathcal{T}_L(k)$  and  $\mathcal{T}_L^{(1)}(k)$  defined as

$$\begin{aligned} \mathcal{T}_L(k) &\equiv \int_{\eta_*}^{\eta_0} d\eta \dot{\tau}(\eta) j_L(k(\eta_0 - \eta)) \\ \mathcal{T}_L^{(1)}(k) &\equiv \int_{\eta_*}^{\eta_0} d\eta \dot{\tau}(\eta) j'_L(k(\eta_0 - \eta)) \end{aligned} \quad (30)$$

where, as defined above,  $\eta_*$  is the epoch at which the visibility function is maximum and  $\eta_0$  is the present epoch. Using these transfer functions in (29) and comparing to (25) allows us to write

$$C_L^{\alpha\alpha} = \frac{2}{\pi} \int \frac{dk}{k} \Delta_M^2(k) \left[ \frac{L}{2L+1} (\mathcal{T}_{L-1}(k))^2 + \frac{L+1}{2L+1} (\mathcal{T}_{L+1}(k))^2 - (\mathcal{T}_L^{(1)}(k))^2 \right] . \quad (31)$$

The function  $\mathcal{T}_L^{(1)}$  can be expressed in terms of  $\mathcal{T}$  functions by using the relation

$$j'_L(x) = \frac{1}{2L+1} [L j_{L-1}(x) - (L+1) j_{L+1}(x)] . \quad (32)$$

This gives

$$\mathcal{T}_L^{(1)} = \frac{1}{2L+1} [L \mathcal{T}_{L-1} - (L+1) \mathcal{T}_{L+1}] . \quad (33)$$

The functions  $\mathcal{T}_L(k)$  are independent of the magnetic field, and can be easily evaluated numerically using the ionization history from CMBFAST.

Eq. (31) is our final result for the FR correlation function. It will be useful in Sec. IV where we find  $C_l^{BB}$  in the thin LSS approximation. However, the result is not useful in the general case of a thick LSS because then  $C_l^{BB}$  is not simply related to  $C_L^{\alpha\alpha}$ .

#### IV. FARADAY ROTATION OF CMB IN THIN LSS APPROXIMATION

In the limit of instant last scattering one assumes that all of the polarization was generated at the peak of the visibility function. Since we are interested specifically in the FR effects, we will neglect primordial tensor modes and any actively sourced vector and tensor modes (including those sourced by magnetic fields) so that only  $E$  mode is produced at the instant of last scattering. At subsequent times, because of the residual presence of charged particles, some of this  $E$  mode will be Faraday rotated into  $B$  mode. To estimate this effect, we can start with Eq. (6) of [40] (same as Eq. (20) of [41]) which gives the B-mode coefficients

$$B_{lm} = 2(-1)^m \sum_{LM} \sum_{l_2 m_2} \alpha_{LM} E_{l_2 m_2} \xi_{lm l_2 m_2}^{LM} H_{ll_2}^L, \quad (34)$$

where  $\xi_{lm l_2 m_2}^{LM}$  and  $H_{ll_2}^L$  are defined in terms of Wigner 3-j symbols as [41]

$$\xi_{lm l_2 m_2}^{LM} \equiv (-1)^m \sqrt{\frac{(2l+1)(2L+1)(2l_2+1)}{4\pi}} \begin{pmatrix} l & L & l_2 \\ -m & M & m_2 \end{pmatrix} \quad (35)$$

$$H_{ll_2}^L \equiv \begin{pmatrix} l & L & l_2 \\ 2 & 0 & -2 \end{pmatrix}, \quad (36)$$

and the summation is restricted to be only over even  $L + l_2 + l$ . From the above, we can derive the expression relating  $C_l^{BB}$  to  $C_l^{EE}$ :

$$\begin{aligned} \langle B_{l'm'}^* B_{lm} \rangle &= 4 \sum_{LM} \sum_{L'M'} \sum_{l_2 m_2} \sum_{l'_2 m'_2} \xi_{lm l_2 m_2}^{LM} H_{ll_2}^L \xi_{l'm' l'_2 m'_2}^{L'M'} H_{l'l'_2}^{L'} \langle \alpha_{LM}^* E_{l_2 m_2}^* \alpha_{L'M'} E_{l'_2 m'_2} \rangle \\ &= \delta_{ll'} \delta_{mm'} 4 \sum_L \frac{(2L+1)}{4\pi} C_L^{\alpha\alpha} \sum_{l_2} (2l_2+1) C_{l_2}^{EE} (H_{ll_2}^L)^2 \end{aligned} \quad (37)$$

which assumes a statistically isotropic stochastic magnetic fields with a FR angular spectrum  $C_L^{\alpha\alpha}$  given by Eq. (31). Therefore, the B-mode angular spectrum in the thin last scattering approximation is

$$C_l^{BB} = \frac{1}{\pi} \sum_L (2L+1) C_L^{\alpha\alpha} \sum_{l_2} (2l_2+1) C_{l_2}^{EE} (H_{ll_2}^L)^2. \quad (38)$$

It is instructive to put the expressions for the CMB observables in a form that separates the well-established physics of FR of CMB polarization from the particular form of the magnetic field spectrum. For example, substituting (31) into (38), we can re-write the latter as

$$C_l^{BB} = \frac{2}{\pi} \int \frac{dk}{k} \Delta_M^2(k) W_l(k), \quad (39)$$

where  $W_l(k)$  are “window functions” defined as

$$W_l(k) = 4 \sum_{l_1 L} \frac{(2l_1+1)(2L+1)}{4\pi} (H_{ll_1}^L)^2 C_{l_1}^{EE} \left( \frac{L}{2L+1} [\mathcal{T}_{L-1}(k)]^2 + \frac{L+1}{2L+1} [\mathcal{T}_{L+1}(k)]^2 - [\mathcal{T}_L^{(1)}(k)]^2 \right). \quad (40)$$

They describe the amount of power a given wavelength  $k$  of the magnetic field spectrum contributes to a given angular scale  $l$  of the B-mode polarization spectrum. We note that Eq. (39) relating  $C_l^{BB}$  to the magnetic spectrum is formally independent of the thin LSS approximation – the approximation is used in the calculation of the window functions. Transfer functions  $\mathcal{T}_L(k)$  can be found numerically using the differential optical depth calculated in CMBFAST [42]. Having evaluated the window functions once, one can store them and use (39) to calculate  $C_l^{BB}$  for different choices of the magnetic spectrum.

#### V. EXACT (THICK LSS) TREATMENT OF FARADAY ROTATION

The thin LSS approximation decouples the process of generation of the CMB polarization by Thomson scattering from its subsequent FR by magnetic fields. It effectively assumes that the background E-mode polarization on all



angular scales was created at a single instant in time corresponding to the peak of the visibility function. While this may suffice for order of magnitude estimates, polarization in different parts of the sky was created at different times and any choice of a single time is essentially arbitrary. Furthermore, the amount of the FR strongly depends on the choice of the initial instant, since the amplitude of the rotation is directly proportional on the rapidly decreasing free electron density. In this Section we derive the exact FR window functions, denoted by  $\tilde{W}_l(k)$ , by solving the radiative transport equations for the generation and propagation of CMB polarization in the presence of FR by stochastic magnetic fields. The form of Eq. (39) relating  $C_l^{BB}$  to the magnetic spectrum will be the same.

The evolution of CMB Stokes parameters is described by Chandrasekhar's radiative transport equations [43]. In the absence of FR, equations for the  $\mathbf{q}$  Fourier mode of linear polarization parameters  $Q$  and  $U$  are [44]

$$\dot{P}_\pm + iq\mu P_\pm = -\dot{\tau}P_\pm + S_\pm, \quad (41)$$

where  $P_\pm(\mathbf{q}, \hat{n}, \eta) = Q \pm iU$ ,  $\hat{n}$  is the direction of the line of sight,  $\mu = \hat{q} \cdot \hat{n}$ , and

$$S_\pm = \dot{\tau}\sqrt{6} \sum_{a=-2}^2 P^{(a)}(\mathbf{q}, \eta) {}_{\pm 2}Y_{2a}(\hat{n}) \sqrt{\frac{4\pi}{5}}. \quad (42)$$

In the above,  ${}_{\pm 2}Y_{lm}(\hat{n})$  are spin-2 spherical harmonics, and  $P^{(a)}(\mathbf{q}, \eta) = [\Theta_2^{(a)} - \sqrt{6}E_2^{(a)}]/10$ , where  $\Theta_2^{(a)}$  and  $E_2^{(a)}$  are the quadrupole moments of the CMB temperature and E-mode polarization for scalar ( $a=0$ ), vector ( $a=\pm 1$ ) and tensor ( $a=\pm 2$ ) modes. Assuming that polarization generated by vector and tensor sources is negligible, we have

$$S_\pm = \dot{\tau}\sqrt{6}P^{(0)}(\mathbf{q}, \eta) {}_{\pm 2}Y_{20}(\hat{n}) \sqrt{\frac{4\pi}{5}}. \quad (43)$$

FR rotates  $Q$  into  $U$ , and  $U$  into  $Q$ , leading to a new term on the right hand of (41) [45]:

$$\dot{P}_\pm + iq\mu P_\pm = -\dot{\tau}P_\pm \mp 2i\omega_B P_\pm + S_\pm. \quad (44)$$

where  $\omega_B(\hat{n}, \eta) = f\dot{\tau}\mathbf{B}(\mathbf{r}) \cdot \hat{n}$ ,  $\mathbf{r} = (\eta_0 - \eta)\hat{n}$ ,  $f = 3\lambda_0^2/(2\pi e)$ , and  $\lambda_0$  and  $\mathbf{B}$  are the *comoving* wavelength and magnetic field strength. The ordinary differential equation (44) has the inhomogeneous solution

$$P_\pm = \int_0^{\eta_0} d\eta \tilde{s}_\pm(\mathbf{q}, \hat{n}, \eta) e^{\mp 2i \int_\eta^{\eta_0} \omega_B d\eta'}, \quad (45)$$

with

$$\begin{aligned} \tilde{s}_\pm &= S_\pm e^{-\tau} e^{-iq\mu(\eta_0 - \eta)} \\ &= -\dot{\tau} e^{-\tau} \sqrt{6} P^{(0)}(\mathbf{q}, \eta) \sum_l (-i)^l \sqrt{4\pi(2l+1)} [\epsilon_l^{(0)}(q(\eta_0 - \eta)) \pm i\beta_l^{(0)}(q(\eta_0 - \eta))] {}_{\pm 2}Y_{l0}(\hat{n}), \end{aligned} \quad (46)$$

and  $\tau \equiv \int_\eta^{\eta_0} d\eta' \dot{\tau}$ . In the above, we used the identity (Eq. (16) of [44])

$$-\sqrt{\frac{4\pi}{5}} {}_{\pm 2}Y_{20}(\hat{n}) e^{i\vec{q} \cdot \hat{n}r} = \sum_l (-i)^l \sqrt{4\pi(2l+1)} [\epsilon_l^{(0)}(qr) \pm i\beta_l^{(0)}(qr)] {}_{\pm 2}Y_{l0}(\hat{n}), \quad (47)$$

with (in what follows we will not need  $\beta_l^{(0)}$ )

$$\epsilon_l^{(0)}(x) \equiv \sqrt{\frac{3}{8} \frac{(l+2)!}{(l-2)!}} \frac{j_l(x)}{x^2}. \quad (48)$$

For small  $\omega_B$ , we can write (45) as

$$P_\pm(\mathbf{q}, \hat{n}) = \int_0^{\eta_0} d\eta \tilde{s}_\pm(\mathbf{q}, \hat{n}, \eta) \left[ 1 \mp 2i \int_\eta^{\eta_0} \omega_B d\eta' \right]. \quad (49)$$

Next, we can use the total angular momentum formalism of [44] to derive an expression for  $C_l^{BB}$  in terms of the magnetic spectrum  $S(k)$ . From Eq. (55) of [44] we have

$$P_\pm(\mathbf{q}, \hat{n}) = \sum_l (-i)^l \sqrt{\frac{4\pi}{2l+1}} \sum_{m=-l}^l \left( E_l^{(m)}(\mathbf{q}) \pm iB_l^{(m)}(\mathbf{q}) \right) {}_{\pm 2}Y_{lm}(\hat{n}), \quad (50)$$



where  $\hat{q} = \hat{z}$ . Note that in Eq. (55) of [44] the sum over  $m$  runs only from  $-2$  to  $2$  because these are the only modes that can be sourced by scalar, vector and tensor fluctuations in the metric. However, the FR effect on the propagation of photons is not via perturbations of the metric tensor. Hence, to stay general, we keep the sum to be over all  $m$  modes. Inverting (50) and using (49) we obtain

$$B_l^{(m)}(\mathbf{q}) = \frac{1}{(-i)^l} \sqrt{\frac{2l+1}{4\pi}} \int d\hat{n} \int_0^{\eta_0} d\eta \dot{\tau} e^{-\tau} \sqrt{6} P^{(0)}(\mathbf{q}, \eta) \\ \times \sum_{l_1} (-i)^{l_1} \sqrt{4\pi(2l_1+1)} [\epsilon_{l_1}^{(0)} ({}_{+2}Y_{l_1 0} [{}_{+2}Y_{lm}]^* + {}_{-2}Y_{l_1 0} [{}_{-2}Y_{lm}]^*)] \int_{\eta}^{\eta_0} \omega_B d\eta', \quad (51)$$

where we have assumed that FR is the only source of B-mode. The angular spectrum  $C_l^{BB}$  can be written in terms of  $B_l^{(m)}(\mathbf{q})$  as [44]

$$(2l+1)^2 C_l^{BB} = 4\pi \int \frac{d^3\mathbf{q}}{(2\pi)^3} \sum_{m=-l}^l \langle B_l^{(m)*}(\mathbf{q}) B_l^{(m)}(\mathbf{q}) \rangle. \quad (52)$$

Introducing  $g(\eta) = \dot{\tau} \exp(-\tau)$  and  $X_{ll_1}^m \equiv {}_{+2}Y_{l_1 0} [{}_{+2}Y_{lm}]^* + {}_{-2}Y_{l_1 0} [{}_{-2}Y_{lm}]^*$ , and substituting (51) into (52) we obtain

$$(2l+1) C_l^{BB} = 4\pi \int \frac{d^3\mathbf{q}}{(2\pi)^3} 6 \int_0^{\eta_0} d\eta g(\eta) \int_0^{\eta_0} d\eta' g(\eta') \langle P^{(0)*}(\mathbf{q}, \eta) P^{(0)}(\mathbf{q}, \eta') \rangle \\ \times \sum_{m=-l}^l \sum_{l_1} \sum_{l_2} (-i)^{l_1} i^{l_2} \sqrt{(2l_1+1)(2l_2+1)} \epsilon_{l_1}^{(0)}(q(\eta_0 - \eta)) \epsilon_{l_2}^{(0)}(q(\eta_0 - \eta')) \\ \times \int d\hat{n} \int d\hat{n}' X_{ll_1}^{m*}(\hat{n}) X_{ll_2}^m(\hat{n}') \langle \int_{\eta}^{\eta_0} d\eta'' \int_{\eta'}^{\eta_0} d\eta''' \omega_B(\eta'', \hat{n}) \omega_B(\eta''', \hat{n}') \rangle. \quad (53)$$

Eq. (27) for the equal time two-point correlation of rotation measure is easily generalized to the unequal time FR correlation case above. Namely, we have

$$\langle \int_{\eta}^{\eta_0} d\eta' \int_{\eta'}^{\eta_0} d\eta'' \omega_B(\eta'', \hat{n}) \omega_B(\eta''', \hat{n}') \rangle = \frac{2}{\pi} \int \frac{dk}{k} \Delta_M^2(k) \sum_L \left( \frac{2L+1}{4\pi} \right) P_L(\hat{n} \cdot \hat{n}') \mathcal{U}_L(k, \eta, \eta'), \quad (54)$$

where

$$\mathcal{U}_L(k, \eta, \eta') = \frac{L}{2L+1} \mathcal{T}_{L-1}(k, \eta) \mathcal{T}_{L-1}(k, \eta') + \frac{L+1}{2L+1} \mathcal{T}_{L+1}(k, \eta) \mathcal{T}_{L+1}(k, \eta') - \mathcal{T}_L^{(1)}(k, \eta) \mathcal{T}_L^{(1)}(k, \eta') \quad (55)$$

and the transfer functions are the same as before, except for the range of the time integration:

$$\mathcal{T}_L(k, \eta) \equiv \int_{\eta}^{\eta_0} d\eta' \dot{\tau}(\eta') j_L(k[\eta_0 - \eta']) \\ \mathcal{T}_L^{(1)}(k, \eta) \equiv \int_{\eta}^{\eta_0} d\eta' \dot{\tau}(\eta') j_L'(k[\eta_0 - \eta']). \quad (56)$$

The  $\mathcal{U}_L$  in (55) can be written as a sum of terms with separated  $\eta$  and  $\eta'$  dependencies:

$$\mathcal{U}_L(k, \eta, \eta') = \sum_{c=1}^3 u_L^{(c)}(k, \eta) u_L^{(c)}(k, \eta'), \quad (57)$$

where

$$u_L^{(1)} = \sqrt{\frac{L}{2L+1}} \mathcal{T}_{L-1}, \quad u_L^{(2)} = \sqrt{\frac{L+1}{2L+1}} \mathcal{T}_{L+1}, \quad u_L^{(3)} = i \mathcal{T}_L^{(1)} \quad (58)$$

We can also relate  $\langle P^{(0)*}(\mathbf{q}, \eta) P^{(0)}(\mathbf{q}, \eta') \rangle$  to the primordial curvature power spectrum  $\Delta^2(q)$  via

$$\langle P^{(0)*}(\mathbf{q}, \eta) P^{(0)}(\mathbf{q}, \eta') \rangle = q^{-3} \Delta^2(q) P^{(0)*}(q, \eta) P^{(0)}(q, \eta'). \quad (59)$$

Putting it all in (53) and integrating over the angular dependence of  $\mathbf{q}$ , we obtain

$$(2l+1)C_l^{BB} = \frac{2}{\pi} \int \frac{dk}{k} \Delta_M^2(k) \sum_{l_1, l_2, L} \sum_{mM} \mathcal{Z}_{l_1 0 l m}^{LM*} \mathcal{Z}_{l_2 0 l m}^{LM} \frac{2}{\pi} \int \frac{dq}{q} \Delta^2(q) \sum_{c=1}^3 d_{l_1 L}^{(c)*}(q, k) d_{l_2 L}^{(c)}(q, k) , \quad (60)$$

where we have defined

$$\mathcal{Z}_{l_1 0 l m}^{LM} = (-i)^{l_1} \sqrt{(2l_1+1)} \int d\hat{n} X_{l_1}^m Y_{LM}^* , \quad (61)$$

and

$$d_{l_1 L}^{(c)}(q, k) = \int_0^{\eta_0} d\eta g(\eta) \sqrt{6} P^{(0)}(q, \eta) \epsilon_{l_1}^{(0)}(q(\eta_0 - \eta)) u_L^{(c)}(k, \eta) . \quad (62)$$

Using the expression for the integral of a product of three spin-weighted spherical harmonics

$$\int d\hat{n} Y_{l_1 m_1}(\hat{n}) Y_{LM}(\hat{n}) Y_{l_2 m_2}(\hat{n}) = \sqrt{\frac{(2l_1+1)(2L+1)(2l_2+1)}{4\pi}} \begin{pmatrix} l_1 & L & l_2 \\ m_1 & M & m_2 \end{pmatrix} \begin{pmatrix} l_1 & L & l_2 \\ -a & -b & -c \end{pmatrix} \quad (63)$$

and the orthogonality property of Wigner 3- $j$  symbols [46], we have

$$\sum_{mM} \mathcal{Z}_{l_1 0 l m}^{LM*} \mathcal{Z}_{l_2 0 l m}^{LM} = 4\delta_{l_1 l_2} \frac{(2l+1)(2l_1+1)(2L+1)}{4\pi} (\mathcal{H}_{l_1}^L)^2 \text{ if } l+l_1+L = \text{even, and 0 otherwise} . \quad (64)$$

Substituting this into (60) we can write

$$C_l^{BB} = \frac{2}{\pi} \int \frac{dk}{k} \Delta_M^2(k) \tilde{W}_l(k) , \quad (65)$$

with

$$\tilde{W}_l(k) = 4 \sum_{l_1 L} \frac{(2l_1+1)(2L+1)}{4\pi} (\mathcal{H}_{l_1}^L)^2 S_{l_1 L}(k) , \quad (66)$$

where  $l+l_1+L = \text{even}$ , and

$$S_{l_1 L}(k) = \frac{2}{\pi} \int \frac{dq}{q} \Delta^2(q) \sum_{c=1}^3 |d_{l_1 L}^{(c)}(q, k)|^2 . \quad (67)$$

The thick LSS window function in Eq. (66) is very similar to the thin LSS window function given by Eq. (40). Noting that

$$C_{l_1}^{EE} = \frac{2}{\pi} \int \frac{dq}{q} \Delta^2(q) \left[ \int_0^{\eta_0} d\eta g(\eta) \sqrt{6} P^{(0)}(q, \eta) \epsilon_{l_1}^{(0)}(q(\eta_0 - \eta)) \right]^2 , \quad (68)$$

we can see that

$$\frac{2}{\pi} \int \frac{dq}{q} \Delta^2(q) \sum_{c=1}^3 |d_{l_1 L}^{(c)}(q, k)|^2 \quad (69)$$

of the thick case becomes

$$C_{l_1}^{EE} \left( \frac{L}{2L+1} [\mathcal{T}_{L-1}(k)]^2 + \frac{L+1}{2L+1} [\mathcal{T}_{L+1}(k)]^2 - [\mathcal{T}_L^{(1)}(k)]^2 \right) \quad (70)$$

of the thin case if the function  $d_{l_1 L}^{(c)}(q, k)$  defined in Eq. (62) is “factorizable”, that is if

$$d_{l_1 L}^{(c)} \rightarrow u_L^{(c)}(k, \eta_*) \int_0^{\eta_0} d\eta g(\eta) \sqrt{6} P^{(0)}(q, \eta) \epsilon_{l_1}^{(0)}(q(\eta_0 - \eta)) . \quad (71)$$

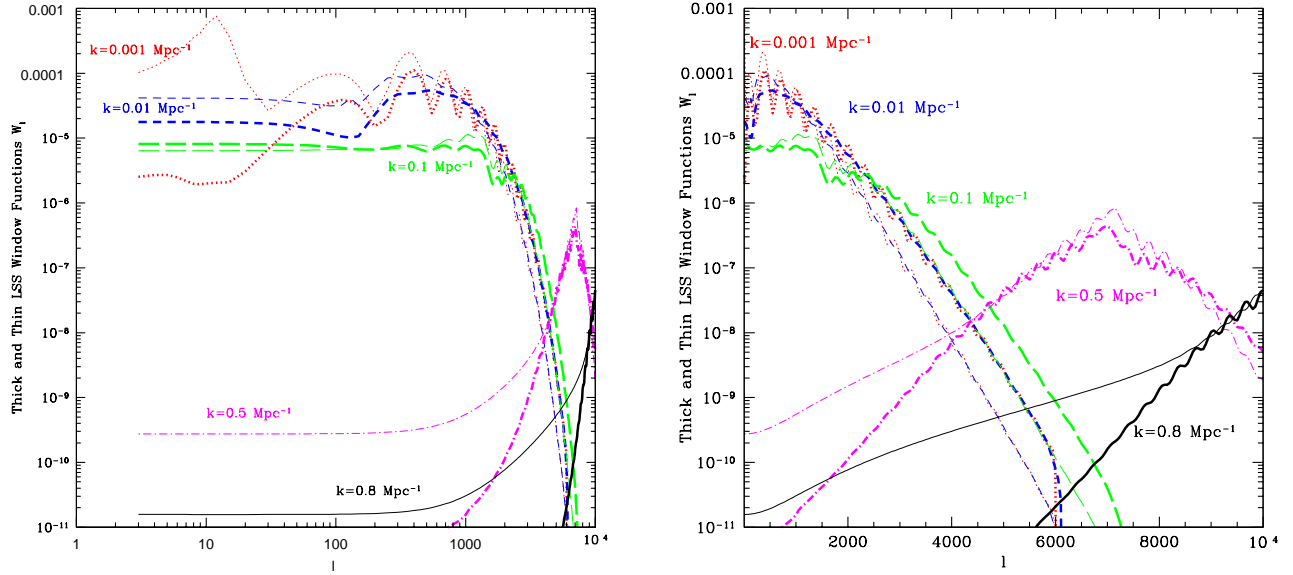


FIG. 2: Window functions  $W_l(k)$  for different values of  $k$  plotted vs  $l$  as evaluated using the full LSS treatment (solid lines) and using the thin LSS approximation (dotted lines). These window functions prescribe the way in which a given Fourier mode  $k$  of the stochastic magnetic field contributes to the multipole  $l$  of  $C_l^{BB}$ . For example,  $C_l^{BB}$  at  $l \sim 8000$  is sensitive to  $\Delta_M^2$  at  $k = 0.5, 1 \text{ Mpc}^{-1}$  but not to smaller  $k$ . The left and right panels show the same functions plotted on logarithmic and linear axis respectively.

Thus the thick LSS case reduces to the thin LSS case if we disregard the convolution in Eq. (62).

The convolution in Eq. (62) will in general not be factorizable, *i.e.* the different  $q$  modes of the source E-mode polarization are not all created at a single time before FR took place. Instead, functions  $d_{l_1 L}^{(c)}(q, k)$  determine the relative amount by which a given  $q$ -mode, projecting into multipole  $l_1$  of  $C_{l_1}^{EE}$ , is distorted by the  $k$ -mode of the magnetic field projecting onto multipole  $L$  of the FR distortion spectrum.

To evaluate  $\tilde{W}_l(k)$  numerically, we modified CMBFAST to calculate sources  $S_{l_1 L}(k)$  on a grid in  $L$  and  $k$ . In order to accurately account for magnetic fields on scales up to a given  $k_{\text{max}}$  in  $\text{Mpc}^{-1}$ , one needs to evaluate the source up to  $L_{\text{max}} \sim (10^4 \text{ Mpc}) k_{\text{max}}$ . We included the  $l_1$  modes up to 6000, and confirmed that it is more than sufficient for all  $k$  and  $L$  because of the exponential suppression of the source E-modes by the Silk damping. Time required for the evaluation of sources needed for  $\tilde{W}_l(k)$  was  $\sim 4000$  CPU-hours, where the sources were sampled for  $450k$  bins. Once the sources are calculated and stored, the sums over  $l_1$  and  $L$  in (66) are quick to perform.

Even though computing the exact window functions  $\tilde{W}_l(k)$  takes a non-trivial amount of CPU time, it only needs to be done once for a given cosmological model. We have made our window functions, evaluated using the  $\Lambda$ CDM model with WMAP7 best fit parameters [47], publicly available at <http://www.sfu.ca/~levon/faraday.html>, along with a Fortran code that calculates  $C_l^{BB}$  for a given  $\Delta_M^2(k)$ .

## VI. RESULTS

In Fig. 2 we show window functions for several values of  $k$  as a function of multipole  $l$  for the thin (dotted lines) and thick (solid lines) LSS treatments discussed in previous sections. These results are independent of the spectral features of the magnetic field. Instead, the role of the window is to specify the extent to which a given Fourier mode

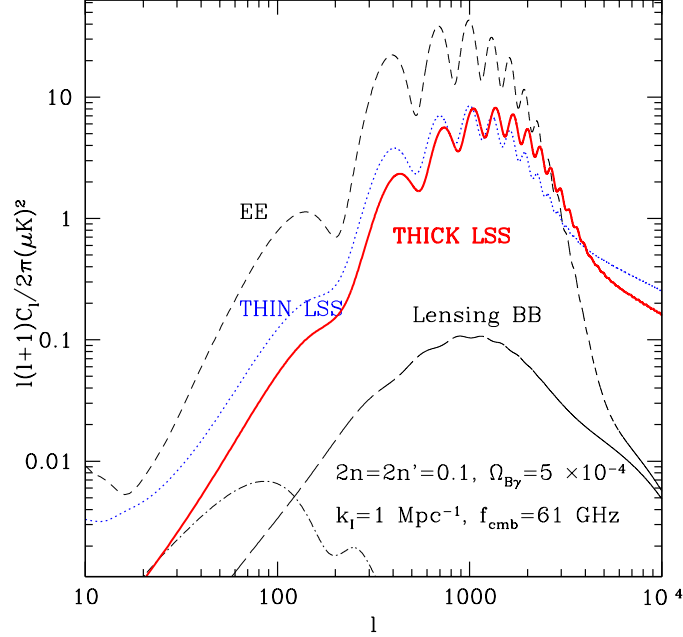


FIG. 3: The CMB B-mode spectrum from Faraday rotation evaluated in the case of a nearly scale-invariant magnetic spectrum with  $2n = 2n' = 0.1$ ,  $k_I = 1 \text{ Mpc}^{-1}$ , and  $f_{\text{cmb}} = 61 \text{ GHz}$ , using the thin (blue dot) and exact (solid red) treatment of LSS. The value of the magnetic field energy fraction  $\Omega_{B\gamma} = 5 \times 10^{-4}$  corresponds to  $B_{\text{eff}} \approx 0.73 \times 10^{-7} \text{ Gauss}$ . The black short-dash line is the input E-mode spectrum, the black dash-dot line is the contribution from inflationary gravitational waves with  $r = 0.1$ , while the black long-dash line is the expected contribution from gravitational lensing by large scale structure.

$k$  of the stochastic magnetic field contributes to the multipole  $l$  of  $C_l^{BB}$ . One can see that each window has a peak at  $l$  approximately given by  $l = 10^4 k$ , where  $10^4$  is roughly the distance to LSS in Mpc. One can also see the oscillations which come from the acoustic oscillations in the E-mode spectrum.

Comparing the exact (thick LSS) windows with the ones obtained in the thin LSS approximation, we note that they have comparable shapes and amplitudes near their peaks, but differ significantly at  $l$  away from the peaks. This difference comes because of the assumption made in the thin LSS approximation that all of the E-mode was produced at the same time, so that the FR occurs at the same rate on all scales. In reality, E-mode is rotated as it is being produced and, since the rate of FR depends on the rapidly decreasing free electron density, E-mode scales produced at different times are rotated at different rates.

Let us now focus on the B-mode spectra for specific choices of the magnetic spectrum. In Fig. 3 we consider a nearly scale invariant magnetic spectrum with  $2n = 0.1$ . The black dash line shows the input E-mode, while the blue dot and the red solid lines show the B-mode spectra obtained using the thin and exact treatment of LSS. One can see that the exactly calculated spectrum favors the power near the peak at the cost of the power around it. Note that in this case the shape of the B-mode is essentially a copy of the E-mode spectrum, except for the lack of exponential damping on small scales. While the EE correlations are suppressed by the Silk damping, there is no exponential suppression of the FR generated small scale B-mode spectrum because the magnetic field is correlated on small scales. For  $2n = 0.1$ , both thin LSS and exact spectra have the asymptotic form of  $l^{-1}$  at high  $l$ . More generally, the asymptotic exponent is  $2n - 1$ , which can be relatively large for stochastic fields *e.g.* for  $n = 5/2$ ,  $l^2 C_l^{BB} \propto l^4$  at large  $l$ .

The Silk damping dissipates the perturbations in the CMB temperature and E-mode on scales smaller than 9 Mpc or so. In our formalism, it comes through the exponential suppression of the source function  $P^{(0)}(k, \eta)$  in Eq. (43).

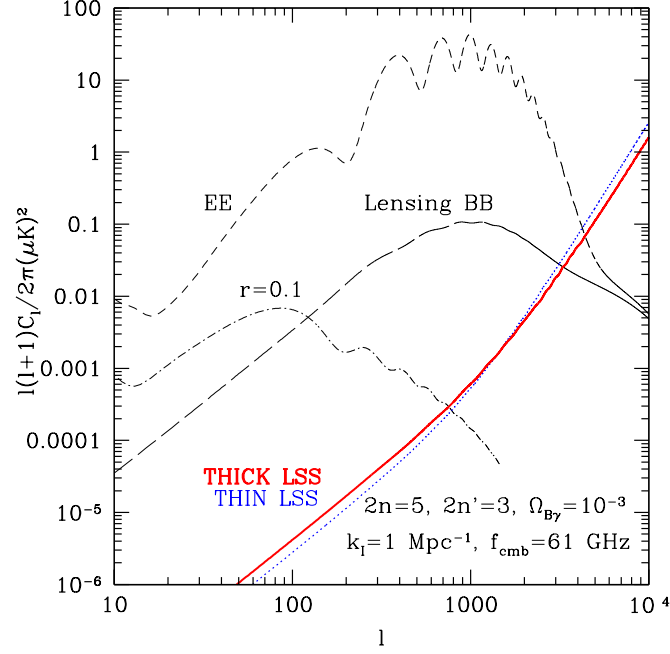


FIG. 4: The CMB B-mode spectrum from Faraday rotation in the  $2n = 5$ ,  $2n' = 3$  case motivated by causally generated fields, with  $k_I = 1 \text{ Mpc}^{-1}$  and  $f_{\text{cmb}} = 61 \text{ GHz}$ . The thin blue dot line shows the thin LSS calculation, while the exact (thick) LSS calculation is shown with solid red. The value of the magnetic field energy fraction,  $\Omega_{B\gamma} = 10^{-3}$ , corresponds to  $B_{\text{eff}} \approx 10^{-7}$  Gauss. The other lines are the same as in Fig. 3.

However, the dissipation scale of (weak) magnetic fields at decoupling time is typically much smaller [13, 34] and for  $k \lesssim 1 \text{ Mpc}^{-1}$  the magnetic field can be treated as a stiff source, *i.e.* we can safely assume that its evolution is independent of the perturbations in the photon-baryon fluid. Then, the only damping of the FR induced B-mode power is due to averaging over many random rotations along the line of sight. The functional form of this suppression is a power law and the exponent can be estimated by observing that a random superposition of  $N$  perturbations along the line of sight leads to a statistical reduction in the amplitude of the observed anisotropy by a factor  $1/\sqrt{N}$ . For wavenumber  $k$  we have  $N \propto \Delta\eta k$ , where  $\Delta\eta$  is the period of time, comparable to the thickness of LSS, during which FR is efficient. Thus, the power spectrum on small scales, which is the square of the FR amplitude, is suppressed by  $1/k$ , which translates into the  $1/l$  suppression of the angular spectrum.

In Fig. 4 we show the plot of the B-mode spectrum for the magnetic spectrum index  $2n = 5$  expected for causally generated magnetic fields [13]. In the figure we used  $k_I = 1 \text{ Mpc}^{-1}$ . For comparison, we show the B-mode from weak lensing and from gravity waves, as well as the E-mode spectrum. Note that at small angular scales (high  $l$ ), the FR produced B-mode can dominate the signal as it keeps growing as  $l^{2n-1}$ .

At present, B-mode have not been detected; there are only upper bounds. Still, even these weak bounds can produce constraints on the magnetic field fraction  $\Omega_{B\gamma}$ , and furthermore, the bounds will improve rapidly as CMB observations are made on smaller angular scales. We derive current constraints on the magnetic field energy density,  $\Omega_{B\gamma}$ , from the WMAP 7-year polarization data by comparing magnetic field induced theoretical CMB B-mode power spectrum  $C_\ell^{BB}$  as given by Eq. (65), with the WMAP observed B-mode power spectrum using the  $\chi^2$  statistics. We consider three WMAP frequency bands Q, V, and W corresponding to frequencies 41 GHz, 61 GHz, and 94 GHz respectively. The lower frequency bands, K and Ka, are foreground dominated and we do not include those in our analysis. We combine

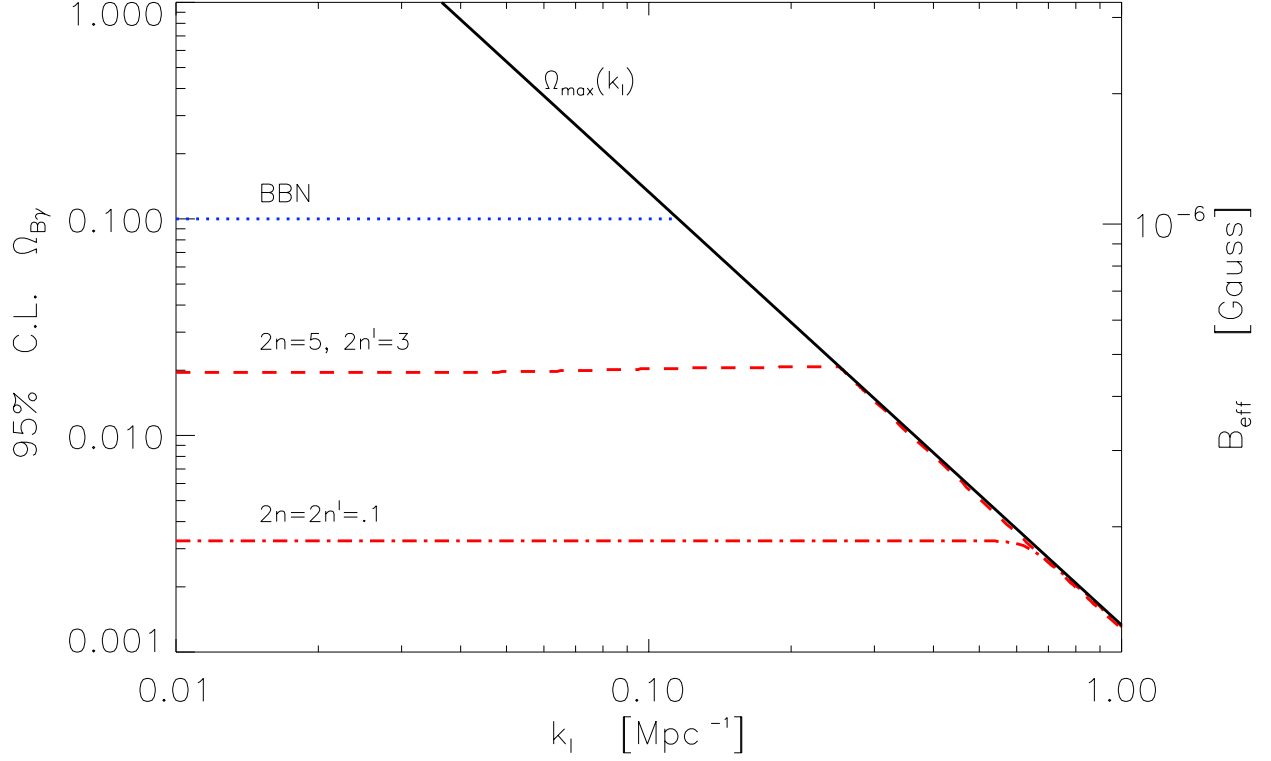


FIG. 5: Constraints from WMAP-7 year data on the magnetic field density  $\Omega_{B\gamma}$ , or analogously magnetic field effective amplitude  $B_{\text{eff}}$  as defined by Eqs. (4) and (17), as a function of the inertial scale wavevector  $k_I$ . We consider two choices of magnetic spectrum, the case of a nearly scale-invariant spectrum  $2n = 2n' = 0.1$  (dash-dot red line) and causal magnetic fields with  $2n = 5, 2n' = 3$  (dashed red line). The BBN constraints on the magnetic field density  $\Omega_{B\gamma} < 0.1$  is shown by the dotted blue line. At large  $k_I$  the bound is set by the theoretical relation between  $\Omega_{B\gamma}$  and  $k_{\text{diss}} \geq k_I$  given by Eq. (15) (black solid line).

different frequency channels directly when evaluating the  $\chi^2$  and, when evaluating the likelihood, we restrict the maximum value of  $\Omega_{B\gamma}$  to the one given by Eq (16) for  $k_I = k_{\text{diss}}$ . We used WMAP data for  $\ell > 32$ , above which the errors for individual  $\ell$ 's can be treated as uncorrelated. The maximum multipole considered in the analysis is  $\ell = 700$ . For our analysis we considered two choices of theoretical magnetic spectral indices  $(n, n')$ , one corresponding to nearly scale-invariant spectrum  $2n = 2n' = 0.1$ , and the other corresponding to causal magnetic fields  $2n = 5, 2n' = 3$ . Our analysis assumes that the magnetic field is the only source of the B-mode signal, and ignores the possibility of other sources of B-modes such as inflationary gravitational waves [48], weak gravitational lensing of the CMB [49], and several other distortions of primary CMB along the line of sight (see Refs. [50, 51] for examples of such distortions).

To obtain bounds on the magnetic field, we note that the CMB FR signature constrains  $\Delta_0^2$  defined in Eq. (14), which is proportional to  $\Omega_{B\gamma}/\kappa$ . Now  $\kappa$  is defined in Eq. (7) and depends on the dissipation scale,  $k_{\text{diss}}$ , which can also be related to  $\Omega_{B\gamma}$  by using Eq. (16). Therefore for given values of  $n$  and  $n'$ ,  $\kappa$  is a function of the inertial scale,  $k_I$ , and the energy fraction in the magnetic field,  $\Omega_{B\gamma}$ . In Fig. 5 we present the 95% confidence level (C.L.) bounds on  $\Omega_{B\gamma}$  for two choices of  $(n, n')$ : the nearly scale-invariant case,  $2n = 2n' = 0.1$ , and the causal case,  $2n = 5, 2n' = 3$ . The bound in each case is presented as a function of  $k_I$ , which we treat as an unknown parameter in the model.

The dependence of the constraint on  $\Omega_{B\gamma}$  on  $k_I$  in each case can be readily understood. In the  $2n = 5, 2n' = 3$  case,  $C_l^{BB}$  is independent of  $k_I$  at very small  $k_I$  because for positive  $n$  the integral in Eq. (65) is dominated by the contribution from  $k \gg k_I$ . The dependence of  $C_l^{BB}$  on  $k_I$  becomes stronger when  $k_I$  gets closer to the range of scales with significant E-mode power ( $k \sim 0.1 \text{ Mpc}^{-1}$ ), which is encoded in the shapes of the window functions. However,

this happens to be just under the maximum wavenumber constrained by WMAP’s measurement of BB. Thus, WMAP is unable to probe the dependence on  $k_I$ , and the constraint line in Fig. 5 stays almost horizontal even at  $k_I \sim 0.1$ . The condition  $k_I \leq k_{\text{diss}} \propto \Omega_{B\gamma}^{-1/2}$  imposes its own upper bound on  $\Omega_{B\gamma}$  at large  $k_I$ . Namely, at sufficiently large  $k_I$ , the constraint curve becomes independent of the CMB constraints, and is a consequence of the constraint arising from dissipation. The curve  $k_I = k_{\text{diss}}$  is also shown in Fig. 5.

In the scale-invariant limit, which is the  $2n = 2n' = 0.1$  case in Fig. 5, the CMB constraint is independent of  $k_I$  because all  $k$  dependence effectively disappears. At large  $k_I$ , the bound is eventually dominated by the  $k_I = k_{\text{diss}}$  curve, which is independent of the CMB data.

We note that a CMB experiment which can measure B-modes at  $\ell \sim 1000$  would be sensitive to changes in  $k_I$  in the case of a causal spectrum. We will present forecasted bounds from future CMB data in an upcoming paper [52].

## VII. CONCLUSIONS

Primordial stochastic magnetic fields may be produced in the early universe during baryogenesis. Characterizing such primordial magnetic field is extremely valuable for probing early universe physics. In this paper we have calculated the effect of primordial magnetic fields on the CMB polarization. This study is especially timely in view of upcoming and next generation of CMB observations that are focused on measuring the polarization of the CMB.

FR of existing E-modes of the CMB can generate parity odd B-modes whose amplitude will depend on the observation frequency bands. We generalized the signatures previously obtained assuming “thin” last scattering surface by solving the full CMB radiative transport equation with FR taken into account. Comparing our full treatment with the thin last scattering approximation, we find the respective B-mode spectra have similar shapes but their magnitudes at a given multipole  $\ell$  may differ by as much as a factor of a few depending on the primordial magnetic field spectrum and the angular scale of observation. The well-established physics of FR of CMB can be encoded in window functions,  $W_l(k)$ , which determine the relative amount that a given Fourier mode  $k$  of the magnetic field contributes to the multipole  $l$  of  $C_l^{BB}$ . The window functions are independent of the details of the magnetic field spectrum and only need to be computed once for a given cosmological model. We have evaluated them in the best fit  $\Lambda$ CDM model and made them available at <http://www.sfu.ca/~levon/faraday.html>, along with a Fortran code that calculates  $C_l^{BB}$  for a given magnetic spectrum.

FR can take a smooth E-mode field and distort it to create B-modes on arbitrarily small scales. For instance, on scales smaller than the Silk damping scale, the E-mode map is essentially homogeneous. However, FR creates E and B-mode inhomogeneities on sub-Silk scales by rotating different parts of the homogeneous E-mode patch in different random ways. As explained in the previous section, the power of these inhomogeneities is suppressed as  $1/l$  due to random superposition of multiple small scale rotations along the same line of sight.

FR of the CMB due to magnetic fields has a distinct frequency dependence ( $\sim \nu^2$ ) which will allow it to be distinguished from other sources of CMB B-modes such as lensing, inflationary gravitational waves, topological defects [53, 54] and FR due to pseudo scalar fields [55–58]. The growth  $l^2 C_l^{BB} \propto l^{2n-1}$  at large  $l$  is *also* characteristic of a magnetic field and *will* help discriminate primordial FR from other foreground contamination. We have summarized current constraints on magnetic energy  $\Omega_{B\gamma}$  from WMAP7 based on the FR induced B-mode spectrum in Fig. 5. For comparison we have also shown the constraints on magnetic energy obtained by BBN. For a scale invariant magnetic field, the constraints from WMAP 7-year data are 2-orders of magnitude better than the BBN constraints. For a causal magnetic field with  $(2n = 5, 2n' = 3)$ , BBN constraints are weaker only by a factor of few. However, note that the constraints from BBN are not expected to improve much in future, but future observations of CMB polarization at smaller angular scales will significantly improve the constraints on magnetic field. We also refer the reader to [59] for the most recent CMB bounds on magnetic fields based signatures other than FR.

Although in this paper we have focused on B-mode power spectrum of CMB generated due to FR of the CMB polarization, recently it has been shown that the stochastic FR of polarization of the CMB couples different CMB angular modes, thus generating non-Gaussianity which can be seen in the CMB trispectrum [40, 41, 60]. In a follow-up paper [52] we discuss the detectability of primordial magnetic field using such non-Gaussian features in the CMB.

## Acknowledgments

We are grateful to the WMAP collaboration, especially Eiichi Komatsu and Michael Nolte, for providing the WMAP B-mode power spectra for individual frequency bands. We thank Karsten Jedamzik, Tina Kahniashvili, and other participants of the Primordial Magnetism Workshop, 2011, at ASU for input, and Richard Battye and Yun Li for pointing out several inconsistencies in the earlier version of the paper. LP is supported by a Discovery Grant from the Natural Sciences and Engineering Research Council of Canada, and acknowledges hospitality at Perimeter



Institute for Theoretical Physics where part of this work was completed. A.P.S.Y. gratefully acknowledges funding support from NASA award number NNX08AG40G and NSF grant number AST-0807444. TV is supported by the Department of Energy at ASU, and is grateful to the Institute for Advanced Study, Princeton (IAS) for hospitality. We also acknowledge the use of cluster computing at the IAS.

- 
- [1] L. M. Widrow, *Rev. Mod. Phys.* **74**, 775 (2002).
  - [2] A. Kandus, K. E. Kunze, and C. G. Tsagas, *Phys. Rep.* **505**, 1 (2011), 1007.3891.
  - [3] A. Neronov and I. Vovk, *Science* **328**, 73 (2010), 1006.3504.
  - [4] T. Vachaspati, *Phys. Lett.* **B265**, 258 (1991).
  - [5] J. M. Cornwall, *Phys. Rev.* **D56**, 6146 (1997), hep-th/9704022.
  - [6] T. Vachaspati, *Phys. Rev. Lett.* **87**, 251302 (2001), astro-ph/0101261.
  - [7] J. Garcia-Bellido, M. Garcia-Perez, and A. Gonzalez-Arroyo, *Phys. Rev.* **D69**, 023504 (2004), hep-ph/0304285.
  - [8] C. J. Copi, F. Ferrer, T. Vachaspati, and A. Achúcarro, *Phys. Rev. Lett.* **101**, 171302 (2008), 0801.3653.
  - [9] T. Vachaspati, *Phil. Trans. Roy. Soc. Lond.* **A366**, 2915 (2008), 0802.1533.
  - [10] Y. Ng and T. Vachaspati, *Phys. Rev.* **D82**, 023008 (2010), 1001.4817.
  - [11] Y. Chu, J. Dent, and T. Vachaspati, *ArXiv e-prints* (2011), 2011.
  - [12] G. Sigl, *Phys. Rev.* **D66**, 123002 (2002), astro-ph/0202424.
  - [13] K. Jedamzik and G. Sigl, *ArXiv e-prints* (2010), 1012.4794.
  - [14] R. Banerjee and K. Jedamzik, *Phys. Rev. D* **70**, 123003 (2004), arXiv:astro-ph/0410032.
  - [15] F. Tavecchio, G. Ghisellini, G. Bonnoli, and L. Foschini (2010), 1009.1048.
  - [16] K. Dolag, M. Kachelriess, S. Ostapchenko, and R. Tomas, *Astrophys. J.* **727**, L4 (2011), 1009.1782.
  - [17] A. Taylor, I. Vovk, and A. Neronov (2011), 1101.0932.
  - [18] K. Takahashi, M. Mori, K. Ichiki, and S. Inoue (2011), 1103.3835.
  - [19] S. Ando and A. Kusenko, *Astrophys. J.* **722**, L39 (2010), 1005.1924.
  - [20] A. Kosowsky and A. Loeb, *Astrophys. J.* **469**, 1 (1996), astro-ph/9601055.
  - [21] D. D. Harari, J. D. Hayward, and M. Zaldarriaga, *Phys. Rev.* **D55**, 1841 (1997), astro-ph/9608098.
  - [22] A. Kosowsky, T. Kahniashvili, G. Lavrelashvili, and B. Ratra, *Phys. Rev.* **D71**, 043006 (2005), astro-ph/0409767.
  - [23] M. Giovannini and K. E. Kunze, *Phys. Rev.* **D78**, 023010 (2008), 0804.3380.
  - [24] T. Kahniashvili, Y. Maravin, and A. Kosowsky, *Phys. Rev.* **D80**, 023009 (2009), 0806.1876.
  - [25] M. Giovannini and K. E. Kunze, *Phys. Rev.* **D79**, 063007 (2009), 0812.2207.
  - [26] R. Durrer and C. Caprini, *JCAP* **0311**, 010 (2003), astro-ph/0305059.
  - [27] M. S. Turner and L. M. Widrow, *Phys. Rev.* **D37**, 2743 (1988).
  - [28] B. Ratra, *Astrophys. J.* **391**, L1 (1992).
  - [29] J. Matese and R. O’Connell, *Nature* **222**, 649 (1969).
  - [30] P. J. Kernan, G. D. Starkman, and T. Vachaspati, *Phys. Rev. D* **54**, 7207 (1996), arXiv:astro-ph/9509126.
  - [31] D. Grasso and H. R. Rubinstein, *Phys. Lett.* **B379**, 73 (1996), astro-ph/9602055.
  - [32] B.-l. Cheng, A. V. Olinto, D. N. Schramm, and J. W. Truran, *Phys. Rev.* **D54**, 4714 (1996), astro-ph/9606163.
  - [33] S. Dodelson, *Modern Cosmology* (Academic Press, San Diego, 2003).
  - [34] K. Jedamzik, V. Katalinic, and A. V. Olinto, *Phys. Rev.* **D57**, 3264 (1998), astro-ph/9606080.
  - [35] T. Kahniashvili, A. G. Tevzadze, S. K. Sethi, K. Pandey, and B. Ratra, *Phys. Rev.* **D82**, 083005 (2010), 1009.2094.
  - [36] D. D. Harari, J. D. Hayward, and M. Zaldarriaga, *Phys. Rev. D* **55**, 1841 (1997), arXiv:astro-ph/9608098.
  - [37] T. A. Enslin and C. Vogt, *Astron. Astrophys.* **401**, 835 (2003), astro-ph/0302426.
  - [38] L. Campanelli, A. D. Dolgov, M. Giannotti, and F. L. Villante, *Astrophys. J.* **616**, 1 (2004), astro-ph/0405420.
  - [39] L. Pogosian, T. Vachaspati, and S. Winitzki, *Phys. Rev. D* **65**, 083502 (2002), arXiv:astro-ph/0112536.
  - [40] M. Kamionkowski, *ArXiv e-prints* (2008), 0810.1286.
  - [41] V. Gluscevic, M. Kamionkowski, and A. Cooray, *Phys. Rev. D* **80**, 023510 (2009), 0905.1687.
  - [42] U. Seljak and M. Zaldarriaga, *Astrophys. J.* **469**, 437 (1996), astro-ph/9603033.
  - [43] S. Chandrasekhar, *Radiative Transfer* (Dover, New York, 1960).
  - [44] W. Hu and M. J. White, *Phys. Rev.* **D56**, 596 (1997), astro-ph/9702170.
  - [45] A. Kosowsky and A. Loeb, *Astrophys. J.* **469**, 1 (1996), astro-ph/9601055.
  - [46] D. A. Varshalovich, A. N. Moskalev, and V. K. Khersonskii, *Quantum theory of angular momentum* (World Scientific, Singapore, 1988).
  - [47] E. Komatsu et al. (WMAP) (2008), 0803.0547.
  - [48] D. Baumann, M. G. Jackson, P. Adshead, A. Amblard, A. Ashoorioon, N. Bartolo, R. Bean, M. Beltrán, F. de Bernardis, S. Bird, et al., in *American Institute of Physics Conference Series*, edited by S. Dodelson, D. Baumann, A. Cooray, J. Dunkley, A. Fraisse, M. G. Jackson, A. Kogut, L. Krauss, M. Zaldarriaga, & K. Smith (2009), vol. 1141 of *American Institute of Physics Conference Series*, pp. 10–120, 0811.3919.
  - [49] K. M. Smith, A. Cooray, S. Das, O. Doré, D. Hanson, C. Hirata, M. Kaplinghat, B. Keating, M. LoVerde, N. Miller, et al., *ArXiv e-prints* (2008), 0811.3916.
  - [50] A. P. S. Yadav, M. Su, and M. Zaldarriaga, *Phys. Rev. D* **81**, 063512 (2010), 0912.3532.

- [51] W. Hu, M. M. Hedman, and M. Zaldarriaga, Phys. Rev. D **67**, 043004 (2003), arXiv:astro-ph/0210096.
- [52] A. Yadav, L. Pogosian, and T. Vachaspati (in preparation).
- [53] U. Seljak, U.-L. Pen, and N. Turok, Phys. Rev. Lett. **79**, 1615 (1997), astro-ph/9704231.
- [54] L. Pogosian and M. Wyman, Phys. Rev. **D77**, 083509 (2008), 0711.0747.
- [55] S. M. Carroll, Phys. Rev. Lett. **81**, 3067 (1998), astro-ph/9806099.
- [56] G.-C. Liu, S. Lee, and K.-W. Ng, Phys. Rev. Lett. **97**, 161303 (2006), astro-ph/0606248.
- [57] M. Pospelov, A. Ritz, and C. Skordis, Phys. Rev. Lett. **103**, 051302 (2009), 0808.0673.
- [58] M. Giovannini and K. E. Kunze, Phys. Rev. **D79**, 087301 (2009), 0812.2804.
- [59] D. Paoletti and F. Finelli, Phys. Rev. D **83**, 123533 (2011), 1005.0148.
- [60] A. P. S. Yadav, R. Biswas, M. Su, and M. Zaldarriaga, Phys. Rev. D **79**, 123009 (2009), 0902.4466.